Low Cycle Fatigue under Multi-axial Stress Conditions

by Koji Mizuhata*

Synopsis

In this paper, low cycle fatigue of the thin-walled cylinder of aluminum alloy 7075-T6 subjected to the combined axial and torsional load has been studied and its applications to the earthquake resistant design of structures have been considered In the experiment, a fatigue machine utilizing the electrohydraulic servomechaniam was constructed. The experimental results showed the linear relationship between the total octahedral shear strain range vs. the number of cycles to fracture on a log-log graph paper. It is shown that these results can be applied to the earthquake resistant design due to the earthquake-like random load.

Nomenclature

$A=\frac{\Delta\sigma}{\Delta\delta}^{xy}$: Ratio between uniaxial and shear strains

dn: Fractional number of cycles at a certain strain level

$d\gamma_{oct}$: Incremental octahedral shear strain amplitude

E, G, ν: Young's modulus, shear modulus, and Poisson's ratio, respectively

h, r: Thickness and radius of the thin-walled cylinder, respectively

k_t, k_s, k_{oct}: Strength coefficients for tension, shear, and octahedral shear, respectively

L: Gage length

M_y, M_u: Yield and ultimate twisting moments, respectively

N, N_t: Numbers of cycles to fracture

n_t, n_s, n_{oct}: Strain-hardening exponents for tension, shear, and octahedral shear, respectively

$p(\gamma_{oct})$: Probability density function

t, t': time, and the time when the stress or strain range is maximum, respectively

α, α_t, α_s, α_{oct}, C, C_t, C_s, C_{oct}: Material constants

$\Delta\varepsilon_{max}$: Maximum principal strain range

$\Delta\varepsilon_p$, $\Delta\gamma_p$: Uniaxial and shear plastic strain ranges, respectively

* Associate Professor of Architectural Engineering, Kobe University, Japan

$\Delta\varepsilon_x$, $\Delta\delta$: Conventional and true axial strain ranges, respectively

$\Delta\sigma_x$, $\Delta\sigma'_x$: Conventional and true axial stress ranges, respectively

$\Delta\tau_{oct}$, $\Delta\gamma_{oct}$: Octahedral shear stress and strain ranges, respectively

$\Delta\tau_{xy}$, $\Delta\gamma_{xy}$: Shear stress and strain ranges, respectively

ΔW: Strain energy per cycle

ε, δ: Conventional and true strains, respectively

ε_f, δ_f: Conventional and true fracture strains, respectively

ε_{if}, γ_f, $\gamma_{oct,f}$: Principal, shear, and octahedral shear fracture strains respectively

ε_x, ε_y, ε_z: Normal strains in x, y, and z directions

θ, θ_f: Angle of twist and fracture angle of twist, respectively

σ, σ': Conventional and true stresses, respectively

σ_i, ε_i: Principal stresses and strains, respectively (i=1, 2, 3)

σ_x, σ_y, σ_z: Normal stresses in x, y, and z directions, respectively

σ_y, σ_u: Yield and ultimate stresses, respectively

τ, γ: Shear stress and strain, respectively

τ_{oct}, γ_{oct}: Octahedral shear stress and strain, respectively

τ_{xy}, τ_{yz}, τ_{zx}, γ_{xy}, γ_{yz}, γ_{zx}: Shear stresses and strains on planes perpendicular to the x, y, and z axes and parallel to the y, z, and x axes, respectively

τ_y, τ_u: Yield and ultimate shear stresses, respectively

ϕ: Phase difference between axial and torsional loads

ω: Circular frequency of cyclic load

Introduction

The fatigue problem has been being treated in the elastic range since long time ago. Recently, however, it becomes necessary to know the behavior of material in the plastic range subjected to large stresses or strains because severe conditions are applied due to the recent technological development. Low cycle fatigue is defined to be the fatigue in which the number of cycles to fracture is from $\frac{1}{4}$ to 10000. In the case of building structures, the members often break due to comparatively few cycles of large fluctuating load, when dynamic loads, such as earthquakes and typhoons are applied. Lately, atomic piles and aircrafts have become to be used in

high temperature and the thermal fatigue problem has been highlighted and followed by the low cycle fatigue problem because of analytical similarity. In the thermal fatigue problem, elongation and contraction caused by temperature change is constrained and the fluctuating stress appears. Therefore, strain becomes meaningful as a parameter. In the low cycle fatigue, since materials go beyond the yield point and get into the plastic region, it may be appropriate to control strain instead of stress. In addition, the material behavior is more stable during strain cycling than during stress cycling. For these reasons, the strain controlled test are usually used in the low cycle fatigue strdies. Based on this fact, Manson and Coffin[1] first proposed the relationship $\Delta\varepsilon_p N^{\alpha}=C$ in the uniaxial test, where $\Delta\varepsilon_p$ is the plastic strain range, N the number of cycles to fracture, and α and C constants. After that, many numbers of experiments have been conducted and various kinds of equations and methods of analysis have been proposed by many investigators. However, these have been done mainly for the uniaxial case and there are few strdies for the multiaxial case. These low cycle fatigue studies have already been reviewed well by some scholars[2)~5)] The fatigue problem may be treated in the following stages according to the scale of the model: (1) Atomic Scale, (2) Crystallograghic Scale, (3) Material Mechanics Scale, (4) Structural Member, and (5) Assembled Structural Model. Although the studies on fatigue have been done in all the above stages, it is not possible to explain completely the behavior in one stage from those in other stages. In this study, the stages (3) and (4) have been considered. The previous studies on low cycle fatigue may be classified as follows: (1) Damages by Sequential Loading, (2) Effect of Mean Stress and Strain, (3) Effect of Multiaxial Stress Conditions, (4) Effects of Temperature and Cyclic Loading Rate, (5) Change of Mechanical Properties during cycling, (6) Effect of Stress Concentration, (7) Bending Fatigue, (8) Size Effect, and (9) Effect of Pattern of Loading. Multiaxial stress states were generated in the previous low cycle fatigue studies as follows: (1) Torsional Cycling or Combined Axial and Torsional Cycling, (2) Bending of Thin Wide Plates, (3) Bending of Circular, Oval, or Rectangular Plates Supported Simply along Eges, (4) Anticlastic Bending of Rhombic Plates, and (5) Combined Axial and Internal Pressure Cycling, etc.. In this study, the biaxial low cycle fatigue where the combined axial and torsional deformations are applied synchronously or nonsynchronously on the thin-walled cylinder of aluminum alloy 7075-T6 is dealt with, and it is considered how to correlate the low cycle fatigue problem with the structural dynamics.

Experimental Studies

Aluminum alloy 7075-T6 was used as material in the experiment. This is a kind of semi-ductile material. Chemical composition of this material is as follows: Al 90.0%, Zn 5.6%, Mg 2.5%, Cu 1.6%, Cr 0.3%. This material is classified crystallographically into the face centred cubic crystal. The mechanical properties of this material according to Ref.(6) and the author's tests are shown as follows: Young's Modulus=10.4×10^6psi, Shear Modulus=3.9×10^6psi, Poisson's Ratio=0.33, Yield Strength=70ksi, Tensile Strength=80 ksi, Elongation in 2in=10%, Hardness H_B=150, Melting Point=1035±145°F, Strain-hardening Exponent=0.11, Strength Coefficient=115700psi. The material used was supplied by an aluminum company with the shape of seamless pipe with the outer diameter of $1\frac{1}{2}$in, the internal diameter of 1in, the wall thickness of $\frac{1}{4}$in, and the length of 3ft.

The specimen used in the experiment is drawn in Fig. 1. The specimen

has the total length of 9½in, the internal diameter of 1in, the gage length of 1in, and the wall thickness of 0.05in in the gage length portion. The specimen has the thread and the key-way in both ends to fix the specimen to the testing machine. The shape of the specimen is determined by copying the plastic torsion specimen of ASTM Standards, so that there occur neither stress gradient in the thickness direction nor static local buckling. The specimens were cut out of the original seamless pipe. Their surface was not polished.

A new testing machine has been constructed so as to conduct the combined axial and torsional low cycle fatigue test. This testing machine can give the specimen synchronously or nonsynchronously the tension-compression and the cyclic torsion independently. The electrohydraulic servomechanism is utilized in this machine and the hydraulic pressure follows the electric input signal. The capacity of this machine is determined by considering those of all machine parts in the whole. As the results, the capability is limited by the hydraulic pump which has the flow capacity of 15gallon per minute under the hydraulic pressure of 2000psi. The cyclic loading rate depends on the input signal moter in this machine. For the rate of 8rpm, the gain is unity and the phase differnce is zero as the results of the system analysis. The machine consists of the following parts: (1) Mechanical part, (2) Electric Part, (3) Hydraulic Part, and (4) Recording Part. The mechanical part is the part to set up the specimen at the specified position and to transmit the hydraulic force controlled electrically to the specimen. The electric part contains the input signal generator, the power supplier, and the servocontroller, etc.. The hydraulic part generates the hydraulic pressure and gives this to the mechanical part. The recording part measures and records the stresses and the strains on the specimen with time. The interrelation among these machine parts is shown in Fig. 2. This machine has two independent channels.

In the experiment, the necessary and sufficient quantities should be read. The following quantities may be considered: For the axial motion, Pressure, Stress, Deformation, and Strain; for torsion, Pressure, Shearing Stress, Twisting Angle, and Shear Strain. For the purpose of energy consideration, these quantities must be read continuously with time. However, if appropriate calibration tests are done statically for each channel, all the above quantities need not to be recorded in the case of cyclic combined test. Measurements and recording were done as follows:

(1) Axial Motion: The pressure was recorded by reading the pressure gage equipped right before the port of the actuator for both tension and compression. The stress were recorded by a pen recorder as the output of the strain gages put on the load cell parallel to its axis. For the strain gage, the axial direction component of a steel compasated resette foil gage was used. The deformation was measured by the dial gage fixed on the die set. The dial gage reading shows the elongation of the total length of the specimen plus the backlash of the thread. This quantity can be read out also as the electric voltage by means of the feedback LVDT(Linear Variable Differential Transformer) fixed on the same die set. The output of the LVDT can be recorded continuously by a cathode-ray oscilloscope with a memory. The strain in the gage length was measured by both the extensometer attached to the specimen and the strain gage and, at the same time, directly by a telescopic gage and a micrometer. The output of the extensometer was

recorded by the pen recorder. In the uniaxial test, the relationship between the extensometer reading and the telescopic gage reading was first plotted for the static test and, then, for the cyclic tests the strains were obtained from the continuous reading of the extensometer by using this diagram. In the combined test, the relationship between the strain range by the strain gage put on the specimen and that by the dial gage was first plotted for the typical tes , and then, for other cyclic tests, the strain range was obtained from the dial gage by using the diagram. For the strain gage put on the specimen, the dynamic post yield foil strain gage was used. The schematic diagram for reading the axial motion is shown in Fig. 3(a).

(2) Torsion: The pressure was read out by using the pressure gages right before the ports of the actuator for both the clockwise and the anticlockwise directions. The shear stress due to torsion was measured by means of four active gage method by using four strain gages put on the load cell in the direction of 45° from the axis and recorded by the pen recorder. For the strain gage the orthogonal component of the same rosette foil strain gage as that for the uniaxial case was used. The twisting angles for the gage length and between the grips can be read out by using the protractor installed on the specimen and the angular scale drawn on the wall of the bearing housing, respectively. Also, the rotary motion can be obtained by converting it into the linear motion by the device attached to the axis of the rotary actuator and then by reading the linear motion by the LVDT. This LVDT is also the feed back transducer for torsion. The output of the LVDT can be read on the cathode-ray oscilloscope. The shear strain can be measured by two strain gages put on the specimen in the direction of 45° from the axis by means of two gage method. For the strain gage, the post yield resette foil gage was used. In the experiment, after it is made sure for the typical test that the strain by the strain gage agrees satisfactorily with that obtained theoretically by the protractor reading of the twisting angle, the strain was determined only by the protractor reading for the other tests. The schematic diagram of the recording system in the torsion test is shown in Fig. 3(b).

The following seventy-six tests were conducted: (1) One Uniaxial Static Test, (2) Twenty-one Uniaxial Fatigue Tests, (3) Two Torsion Static Tests, (4) Nineteen Torsion Fatigue Tests, (5) One Combined Axial and Torsional Static Test, (6) Eight Combined Axial and Torsional Synchronous Fatigue Tests with the Strain Ratio $A=\Delta\gamma_{xy}/\Delta\delta=2$, (7) One Combined Axial and Torsional Static Test with the Strain Ratio A=1, (8) Three Combined Axial and Torsional Synchronous Fatigue Tests with the Strain Ratio A=1, (9) One Combined Axial and Torsional Static Test with the Strain Ratio A=3, (10) Three Combined Axial and Torsional Synchronous Fatigue Tests with the Strain Ratio A=3, (11) Eight Combined Axial and Torsional Nonsynchronous Fatigue Tests with the Strain Ratio A=2 and the Phase Difference $\phi=90°$, and (12) Eight Combined Axial and Torsional Nonsynchronous Fatigue Tests with the Strain Ratio A=2 and the Phase Difference $\phi=45°$. These tests were planed according to the following idea: In order to compare the previous results with the same material, the range of the number of cycles to fracture has been selected to be from $\frac{1}{4}$ to 2000. Except the uniaxial tests which include the preliminary tests for the purpose of watching how accurate the machine worked, four or five strain levels were chosen and on each strain level three tests were conducted. For the combined tests, the ratio of the axial and the torsional strains of 1:2(A=2) and the phase difference of

zero (ϕ=0) were selected as the standard case. The strain ratio of 1:2 gives the same damage to both the axial and torsional strain gage if one uses the three element right angled rosette strain gage. The strain ratios were taken 1:1, 1:2, and 1:3, and the phase difference were 0°, 45°, and 90° With the expectation that the test results for different ratios may appear on the straight line on the log-log plot of the octahedral shear strain vs. the number of cycles to fracture, only four tests on different levels including the static test were conducted for each ratio of strains. For the phase differences other than 0°, that is, nonsynchronous case, the strain ratio was selected to be 1:2 only, to know only the effect of phase difference. For this series, two specimens, one of which has a strain gage, were tested for each strain level. Besides the above mentioned plan, a small number of arbitrary variations were added.

Analysis of Experimental Results and Discussions

In the following, the experimental results are analyzed, plotted, and then discussed.

(1) Uniaxial Test

(a) Uniaxial Static Test (Tension Test). The uniaxial static test gives the basic data of the material. Both the conventional and true stress-strain curves are plotted by both the regular and the log-log scales. The stress was calculated from the output of the strain gage put on the load cell. The strain was calculated from the output of the strain gage put on the specimen. The origin of the stress-strain curve was adjusted. The true stress was calculated by the formula $\sigma'=\sigma(1+\varepsilon)$, and the true strain was calculated by the formula $\delta=\log_e(1+\varepsilon)$, where σ and σ' represent the conventional and the true stresses, respectively, and ε and δ the conventional and the true strains, respectively. From the conventional stress-strain curve, the following basic data of the material have been obtained: Young's Modulus $E=9\times10^6$psi, Yield Strength σ_y=71ksi, Tensile Strength σ_u= 81.5ksi; Ductility ε_f=12%, δ_f=11.1%. From the log-log true stress-strain line the material constants have been obtained as below: Strain-hardening Exponent n_t=0.109, Strenth Coefficient k_t=115700psi.

(b) Uniaxial Fatigue Tests. Twenty-one fatigue tests were conducted including the static test which corresponds to $N=\frac{1}{4}$, $\Delta\delta=2\varepsilon_f$, where N represents the number of cycles to fracture vs. the true strain range are plotted on the log-log graph paper as shown in Fig. 4. The strain range was obtained from the range of the extensometer reading by extraporating the static range in the calibration diagram between the extensometer reading and the micrometer reading of the telescopic gage. The octahedral shear strain range has been calculated by $\Delta\gamma_{oct}=\sqrt{2}\Delta\delta$. These are plotted later in Fig. 6 with the combined case. Fracture is defined to be the abrupt considerable reduction of stress on the pen recorder when the pretty big sound is heard. Crack propagated from 70%~90% of number of cycles to fracture. However, no considerable stress reduction could not be seen on the pen recorder during the crack propagation. Position of the crack initiation was not definite for lower cycles, while for higher cycles the crack initiated on the boundary between the straight portion and the curved portion. This may be because of the stress concentration. In Fig. 4, the experimental points are connected into one straight line given by $\Delta\delta N_t^{\alpha_t}=C_t$, where α_t=0.24 (0.28 if $N=\frac{1}{4}$ is included) and C_t=0.10 (0.13). For the cycles less than about 100, the experimental points are found to drop below the line. This is because

of the fact that the buckling mode appeared after some number of cycling and this mode became bigger and bigger, therefore, the real local strain became higher than calculated from the die set movement. On the other hand, Manson and Hirschberg[7] got α_t=0.5. The discrepancy may be caused by how to obtain the true strain. In this study, the true strain is rather averaged along the gage length because the strain was calculated from the die set movement, while in Manson-Hirschberg's work, the local true strain was directly measured from the reduction of area. The cyclic hysteresis loop is plotted. The third cycle of N=39 has been chosen, because for earlier cycle the loop is not stable, while for later cycle the strain gage is deteriorated. According to Morrow[8], the stress-strain curve become stable in the cycles less than several percent of number of cycles to fracture. In the cyclic hysteresis loop, the cyclic strain-hardening exponents were calculated to be 0.35 for tension and 0.21 for compression.

(2) Torsion Test

(a) Static Torsion Test. Two static tests were done. The torsion stress-strain curve has been drawn for one of them in which the better strain gage was used. This curve was drawn in the regular and the log-log scales. By this test, the following results have been obtained: Shear Modulus G=3.36×10^{6}psi (observed), or 3.38×10^{6}psi (calculated from the Young's Modulus), Yield Stress τ_y=34800psi, Ultimate Stress τ_u=43700psi, Fracture Strain γ_f=0.38, Yield Twisting Moment M_y=3012lb-in, Ultimate Twisting Moment M_u=3784lb-in, Fracture Angle of Twist θ_f=0.806rad (41°), Strain-hardening Exponent n_s=0.124, and Strength Coefficient k_s=56600 psi. The shear stress was obtained from the strain gages put on the load cell and the smaller shear strains from the strain gage put on the specimen. The fracture angle of twist was read by the protractor set up between the gage length, and then, from this value, the fracture strain was calculated. For the large angle of twist, the shear strain obtained from the rosette strain gage does not show the real value, therefore, the strain was calculated from the observed angle of twist by the formula $\gamma=r\theta/L$, where γ denote the shear strain, r the radius of the specimen, θ the angle of twist, and L the gage length. The twisting moment has been calculated the obtained shear stress by the formula $M_t=2\pi r^2 h\tau$. This was checked by the moment obtained from the pressure gage set up at the pressure ports of the rotary actuator. The shear modulus obtained from the experimental stress-strain curve has been compared with the calculated value from the Young's modulus obtained from the tension test by the formula $G=E/2(1-\nu)$. The negative slope of the stress-strain curve after the maximum stress is reached seems to be because of twisting buckling caused by the principal compressive strain. The octahedral shear strain at fracture, also, has been calculated for the purpose of comparing with other states of strain and is plotted on Fig. 6.

(b) Torsion Fatigue Test. Nineteen torsion tests including two static torsion tests were conducted. Two of them resulted to run out. The shear strain ranges vs. the number of cycles to fracture have been plotted in Fig. 5 in the log-log scale. The octahedral and principal strains were calculated by $\Delta\gamma_{oct}=\sqrt{6}\Delta\gamma_{xy}/3$ and $\Delta\varepsilon_{max}=\Delta\gamma_{xy}/2$, respectively. The shear strain range was calculated from the angle of twist read on the protractor between the gage length. Relationship between the shear strain and the angle of twist was also calibrated in the static test. In Fig. 5 a linear relationship between the shear strain range and the number of cycles to fracture in the log-log scale has been obtained as $\Delta\gamma_{xy}N^{\alpha_s}=C_s$, where α_s=0.34 (0.38) and

C_s=0.32 (0.41). Fracture is determined by considerable reductuion of stress. Previously, Halford and Morrow[9] obtained the expression as $\Delta\gamma_p N^{\frac{1}{2}}=C$ for the solid specimen of 75S aluminum alloy, where $\Delta\gamma_p$ denotes the plastic shear strain range. For low cycle range, the difference between total and plastic strains is negligible. The discrepancy of these slopes may be caused by the buckling mode of tubler specimen. Crack initiated at the crossing point of two hills caused by the compressive principal stress for large strain and crack propagated along the direction of axis for all torsional tests. The octahedral shear strain ranges vs. the number of cycles to fracture are plotted in the log-log scale later in Fig. 6 to compare other strain conditions. A typical cycling shear stress-strain curve is plotted. From this curve, the cyclic strain-hardening exponent are obtained to be n_s=0.21 and 0.27. Stress and strain were obtained from the strain gages.

(3) Derivation of the Principal Stress and Strain and the Octahedral Shear Stress and Strain for the Combined Axial and Torsional Case.

For the combined axial and torsional case, the strain states are

$$\varepsilon_x=\varepsilon_x,\ \varepsilon_y=-\tfrac{1}{2}\varepsilon_x,\ \varepsilon_z=-\tfrac{1}{2}\varepsilon_x,\ \gamma_{xy}=\gamma_{xy},\ \gamma_{yz}=\gamma_{xz}=0, \tag{1}$$

from which the principal strains become

$$\varepsilon_1=\tfrac{1}{4}\varepsilon_x+\tfrac{1}{4}\sqrt{9\varepsilon_x^2+4\gamma_{xy}^2},\ \varepsilon_2=\tfrac{1}{4}\varepsilon_x-\tfrac{1}{4}\sqrt{9\varepsilon_x^2+4\gamma_{xy}^2},\ \varepsilon_3=-\tfrac{1}{2}\varepsilon_x. \tag{2}$$

The octahedral shear strain for the general case is

$$\gamma_{oct}=\tfrac{2}{3}[(\varepsilon_1-\varepsilon_2)^2+(\varepsilon_2-\varepsilon_3)^2+(\varepsilon_3-\varepsilon_1)^2]^{1/2}. \tag{3}$$

For the biaxial case, under consideration of incompressibility, $\varepsilon_1+\varepsilon_2+\varepsilon_3=0$, Expression (3) turns out as

$$\gamma_{oct}=\tfrac{2\sqrt{6}}{3}[\varepsilon_1^2+\varepsilon_1\varepsilon_2+\varepsilon_2^2]^{1/2}. \tag{4}$$

Substituting Expression (2) into Expression (4), one gets

$$\gamma_{oct}=\tfrac{\sqrt{6}}{3}[3\varepsilon_x^2+\gamma_{xy}^2]^{1/2}. \tag{5}$$

During cycling, the strains are expressed by

$$\varepsilon_x=\Delta\varepsilon_x\sin\omega t,\ \gamma_{xy}=\Delta\gamma_{xy}\sin(\omega t+\phi). \tag{6}$$

Substituting Eq.(6) into Expression (5), one obtains

$$\gamma_{oct}=\tfrac{\sqrt{6}}{3}[3\Delta\varepsilon_x^2\sin^2\omega t+\Delta\gamma_{xy}^2\sin^2(\omega t+\phi)]^{1/2}. \tag{7}$$

In order to get the time when the octahedral shear strain becomes maximum, one lets $d\gamma_{oct}/dt=0$, then

$$\tan2\omega t'=-\Delta\gamma_{xy}^2\sin2\phi/(3\Delta\varepsilon_x^2+\Delta\gamma_{xy}^2\cos2\phi). \tag{8}$$

For the synchronous case, ϕ=0, the octahedral shear strain is maximum, when $\sin\omega t$ is maximum. For ϕ=90°, Eq.(8) turns out as $\tan2\omega t'=0$, then $\omega t'$=0°, 90°, 180°, ... For $\sqrt{3}\Delta\varepsilon_x>\Delta\gamma_{xy}$, the maximum occurs when $\omega t'$=90°, 270°,.... and the maximum value $\gamma_{oct,max}=\sqrt{2}\Delta\varepsilon_x=1.414\Delta\varepsilon_x$ and at this time, $\varepsilon_{1,2}=\Delta\varepsilon_x$, $\Delta\varepsilon_x/2$. For $\sqrt{3}\Delta\varepsilon_x<\Delta\gamma_{xy}$, the maximum occurs when $\omega t'$=0°, 180°,.... and the maximum value is $\gamma_{oct,max}=\tfrac{\sqrt{6}}{3}\Delta\gamma_{xy}=0.816\Delta\gamma_{xy}$, and at this time, $\varepsilon_{1,2}=\pm\Delta\gamma_{xy}/2$. For ϕ=45°, Eq.(8) turns out as $\tan2\omega t'=-\Delta\gamma_{xy}^2/\Delta\varepsilon_x^2$ and at this time

$$\gamma_{oct,max}=\tfrac{\sqrt{2}}{3}[3\Delta\varepsilon_x^2(1-\cos2\omega t')+\Delta\gamma_{xy}^2(1+\sin2\omega t')]^{1/2}, \tag{9}$$

$$\varepsilon_{1,2}=\sqrt{2}[\Delta\varepsilon_x\sqrt{1-\cos2\omega t'}\pm\sqrt{9\Delta\varepsilon_x^2(1-\cos2\omega t')+4\Delta\gamma_{xy}^2(1+\sin2\omega t')}]^{1/2}/8. \tag{10}$$

$\omega t'$ should be carefully chosen so as γ_{oct} is maximum. For the true strain expressions, one has only to change ε into δ.

For the combined axial and torsional case, the stress states are

$$\sigma_x=\sigma_x,\ \tau_{xy}=\tau_{xy},\ \sigma_y=\sigma_z=\tau_{yz}=\tau_{zx}=0, \tag{11}$$

then the principal stresses are

$$\sigma_1=\tfrac{1}{2}\sigma_x+\sqrt{(\tfrac{1}{2}\sigma_x)^2+\tau_{xy}^2},\ \sigma_2=\tfrac{1}{2}\sigma_x-\sqrt{(\tfrac{1}{2}\sigma_x)^2+\tau_{xy}^2},\ \sigma_3=0. \tag{12}$$

The octahedral shear stress for the general case is

$$\tau_{oct}=\tfrac{1}{3}[(\sigma_1-\sigma_2)^2+(\sigma_2-\sigma_3)^2+(\sigma_3-\sigma_1)^2]^{1/2}. \tag{13}$$

For the biaxial case, Expression (13) turns out as

$$\tau_{oct}=\frac{\sqrt{2}}{3}[\sigma_1^2+\sigma_2^2-\sigma_1\sigma_2]^{1/2}. \quad (14)$$

Substituting Expression (12) into Expression (14), one obtains

$$\tau_{oct}=\frac{\sqrt{2}}{3}[\sigma_x^2+3\tau_{xy}^2]^{1/2}. \quad (15)$$

During cycling, the stresses are expressed by

$$\sigma_x=\Delta\sigma_x\sin\omega t,\ \tau_{xy}=\Delta\tau_{xy}\sin(\omega t+\phi). \quad (16)$$

Substituting Eq.(16) into Expression (15), one obtains

$$\tau_{oct}=\sqrt{2}[\Delta\sigma_x^2\sin^2\omega t+3\Delta\tau_{xy}^2\sin^2(\omega t+\phi)]^{1/2}/3. \quad (17)$$

In order to get the time when the octahedral shear stress becomes maximum, one lets $d\gamma_{oct}/dt=0$, then

$$\tan 2\omega t'=-3\Delta\tau_{xy}^2\sin 2\phi/(\Delta\sigma_x^2+3\Delta\tau_{xy}^2\cos 2\phi). \quad (18)$$

For the synchronous case, $\phi=0$, the octahedral shear stress is maximum, when $\sin\omega t$ is maximum. For $\phi=90°$, Eq.(18) turns out as $\tan 2\omega t'=0$. For $\Delta\sigma_x>\sqrt{3}\times\Delta\tau_{xy}$, the maximum occurs when $t=90°, 270°, \ldots$, and the maximum value $\tau_{oct,max}=\frac{\sqrt{2}}{3}\Delta\sigma_x$. For $\Delta\sigma_x<\sqrt{3}\Delta\tau_{xy}$, the maximum occurs when $t=0°, 180°, \ldots$, and the maximum value $\tau_{oct,max}=\frac{\sqrt{6}}{3}\Delta\tau_{xy}$. For $\phi=45°$, Eq.(18) turns out as $\tan 2\omega t'=-3\Delta\tau_{xy}^2/\Delta\sigma_x^2$. In general, the time for the maximum octahedral shear stress and strain do not coincide.

(4) Combined Axial and Torsional Synchronous Test

(a) Static Combined Test. Three static combined tests were done. One of them has the axial and shear strain ratio of 1:2; one does that of 1:3; the other does that of 1:1. The important data in these tests as the basis of fatigue test are the fracture stress and strain, which are expressed by means of the octahedral shear stress and strain or the principal stress and strain, and the strain data are obtained as

$\gamma_{oct,f}=0.274$, $\varepsilon_{1f}=0.191$, $\varepsilon_{2f}=-0.129$, $\varepsilon_{3f}=-0.061$ for the ratio of 1:2,

$\gamma_{oct,f}=0.171$, $\varepsilon_{1f}=0.121$, $\varepsilon_{2f}=-0,067$, $\varepsilon_{3f}=-0.054$ for the ratio of 1:1,

and $\gamma_{oct,f}=0.281$, $\varepsilon_{1f}=0.195$, $\varepsilon_{2f}=-0.131$, $\varepsilon_{3f}=-0.064$ for the ratio of 1:3.

These data have been plotted with the fatigue data in Figs. 6, 7, and 8. The octahedral shear stress-strain curve for the strain ratio of 1:2 have been plotted in the regular and the log-log scales as a reference. The strain-hardening exponent and the strength coefficient have been obtained from this curve as $n_{oct}=0.117$ and $k_{oct}=50357$psi. These values are compared with the value calculated from the static tension test as follows: $n_{oct}=0.109$, $k_{oct}=52600$psi. The principal and octahedral stress and strain were calculated by using Eqs.(12), (2), (17), and (7) from the axial true stress and strain and the torsional shear stress and strain obtained from the strain gages put on the load cell and the specimens, respectively. The calibration diagram showing the relationship between the die set movement and the axial strain gage reading has been used for obtaining the strain from the die set movement in the combined fatigue tests. On the other hand, regarding the relationship between the angle of twist and the shear strain, a theoretical curve was used, because the theoretical and experimental lines coincide. The failure lines on the specimen in these tests were seen to have the larger angle from the axis of the specimen for the larger strain ratio, that is, the axial strain is larger.

(b) Fatigue Tests with the Strain Ratio A=2. Ten available tests including two static tests were conducted. One of the two static tests could not reach fracture because of unexpectable electric power break, but it went beyond the strain gage ability. Results of these ten tests have been plotted on the log-log graph paper in Fig. 6 to show the relationship between the octahedral shear strain range and the number of cycles to fracture. The relationship between the maximum principal strain range and the

number of cycles to fracture are also shown in Fig. 7. The principal and octahedral shear strain ranges have been calculated from the axial and torsional strain by using the expressions (2) and (12). The axial and torsional shear strain ranges were obtained from the diagrams between the die set movement and the strain and those between the angle of twist and the shear strain, respectively. Both in Figs. 6 and 7 the octahedral shear strain ranges vs. the number of cycles to fracture for the tension test and the torsion test are also plotted to compare the effect of strain state. Goto's data for the rhombic specimens[10] and Shewchuk's data for the oval plate specimens[11] are also plotted in Fig. 6. These results drop exactly on the torsion fatigue data in this study. For the combined case the octahedral shear strain range vs. the number of cycles to fracture has appeared a straight line with the slope of 0.23 (0.36 including $N=\frac{1}{4}$). While for the axial fatigue tests, the slope is 0.24 (0.28) and for the torsion fatigue test, the slope is 0.34 (0.38). These discrepancies of the slopes for three kinds of tests are found larger for lower than about 100cycles than for higher cycles. This may be because of the complexity of the fracture mode in the lower cycles, that is, for the combined case in the low cycle range, the fracture initiated at the crossing points of the two hills of buckling in the compressive direction, when it was applied by tension. Therefore, the local strain seemed to be much larger than the average strain calculated from the die set movement and the twisting angle or the strain gage with the length of $\frac{1}{4}$in. This may be one of the reasons why the maximum principal strain range has less scatter than the octahedral shear strain range does in lower cycles. Another reason of the discrepancy is the definition of the axial true strain like as mentioned in the tension test. After the crack initiated the specimens were torn obliquely. The fracture was determined when the stress reduced considerably. This occurred at the same time as the specimen was torn.

(c) Fatigue Tests with the Ratios A=1 and 3. For each strain ratio, four fatigue tests including one static test were conducted. The results have been plotted on the log-log graph paper in Fig. 8 to show the relationship between the octahedral shear strain range and the number of cycles to fracture for both ratios. The process dealing with the experimental data was the same as in the case of the ratio A=2. In Fig. 8, the log-log plots of the octahedral shear strain range vs. the number of cycles to fracture for both cases appear straight lines with almost the same slopes 0.19 for A =1 and 0.22 for A=3. Comparing these two lines to the line for the ratio A =2, the lines for the ratios A=1 and 3 almost coincide with the line for A =2. Consequently, the effect of strain ratio is found to be negligible, if one uses the octahedral shear strain range. Variation of the principal strain state for the combined axial and torsional case is from $1:-\frac{1}{2}:-\frac{1}{2}$ for the uniaxial case to 1:-1:0 for the torsional case and it is not so large. The modes of fracture for three different ratios of the axial and torsional strains are naturally different. For smaller value of strain ratio A, the fracture line is almost the same as the uniaxial case where it is perpendicular to the axis of the cylinder. For larger value of strain ratio, the main crack was similar to the torsional case and the subsequent crack appeared oblique. The crossing hills by compressive strain was also observed.

(5) Nonsynchronous Fatigue Tests with the Strain Ratio A=2

Two phase differences of 45° and 90° between the axial and torsional

strains have been chosen. Since there is no difference in the biaxial behavior between clockwise and anticlockwise twisting, the phase difference of 180° gives the same effect as that of 360° does. The phase difference means that the twisting angle is ahead the zero axial deformation by the angle of ϕ. The static angle of twist of ϕ was given the specimen prior to the static axial load. Eight fatigue tests have been done for each phase difference. The results have been plotted on the log-log graph paper in Fig. 9 to show the relationship between the octahedral shear strain ranges and the number of cycles to fracture. In Fig. 9, the results for the phase difference of zero which is the synchronous case are, also, plotted for the purpose of comparison. The octahedral shear strain was calculated from the axial strain range and the torsional shear strain range by using Eq.(12). In Fig. 9, the plots are connected into straight lines for both cases. However, some discrepancy can be seen among three lines. The slopes are measured to be 0.18 for 45° and 0.21 for 90°, which are compared to the slope for the synchronous tests. The line for 45° lies below that for the synchronous case and further the line for 90° lies below that for 45° if one takes $\gamma_{oct,max}$ calculated by Eq.(9) along the ordinates. As far as one uses $\gamma_{oct,max}$ derived in Eq.(9), this can not neglect the phase difference. On the other hand, for instance, if the total energy to fracture vs. the number of cycles to fracture have been plotted on the log-log graph paper as shown in Fig. 10, for all the phase differences of 0°, 45°, and 90°, this diagram shows no distinct discrepancy caused by the phase difference, although scatter is large. In this case, the energy was obtained by adding the areas of both the axial and the torsional shear stress-strain hysteresis loops which were recorded by the strain ranges on the load cell and the specimen. In this case, the steady hysteresis loop was selected. The area inside the hysteresis loop, i.e., the dissipated energy can be a parameter but can not be explained theoretically yet. Regarding the mode of fracture, the crack propagated in zig-zag way, that is the crack perpendicular to the axis first, the oblique crack subsequently. In some specimen for ϕ=45°, the cracks were seen everywhere on the gage length.

Low Cycle Fatigue Problems in Earthquake Resistant Design

During earthquake, randomly varying loads are applied on structural members. In this case, the random loads are not direct earthquake motion, but response of the vibrating system with such restoring force characteristics as related to the hysteresis curve of the material, itself. Therefore, the analysis of randomness should be done about the response. Up to the present, there are pretty many studies on high cycle fatigue under randomly varing loads[12], but only a few on low cycle fatigue. Since the structural members often go into the plastic region during large earthquake, low cycle fatigue is more important than high cycle fatigue for the earthquake resistant problem. In order to apply the random fatigue theory for high cycle to low cycle, the stress range for high cycle fatigue has to be rewriten into the strain range for low cycle fatigue. Further, since the strain state in structural members is usually the combined one, the octahedral shear strain, for instance, has to be used as the parameter. With the above-mentioned in mind, the following assumptions are laid in the application of random fatigue theory to the earthquake resistant problem: (1) The linear damage hypothesis is approximately applicable, (2) During cycling, almost steady stress-strain hysteresis curve is hold; in other words, the mechanical properties of the material is not much changed, (3) Effect of the cycling rate is small in low cycle fatigue, (4) Random process is stationary and damage

by non-stationary mean strain is arithmetically added to that by the stationary fluctuating strain. The purpose of the study is to estimate the life of the structural member under the randomly varying load of γ_{oct}~t from the results of tension test and γ_{oct}~N relationship obtained from the constant amplitude test. For the randomly varying strain, the linear damage hypothesis is expressed by

$$\int \frac{dn}{N} = 1 \tag{19}$$

where dn is the number of cycles at a strain level between γ_{oct} and $\gamma_{oct}+d\gamma_{oct}$. Let $p(\gamma_{oct})d\gamma_{oct}$ be the pobability that a given strain cycle will have an amplitude between γ_{oct} and $\gamma_{oct}+d\gamma_{oct}$. This probability will be obtained by using one of the counting methods in Ref.(13) from γ_{oct}~t curve. Then, the number of cycles dn will be given in terms of the total number of cycles N_t by

$$dn=N_t p(\gamma_{oct})d\gamma_{oct} \tag{20}$$

$$\int \frac{N_t p(\gamma_{oct})d\gamma_{oct}}{N} = 1 \tag{21}$$

By the linear relationship of γ_{oct}~N on the log-log paper, one has

$$\Delta\gamma_{oct} N^{\alpha}=\Delta\gamma_{1oct} N_1^{\alpha} \tag{22}$$

Substituting N of Eq.(22) into Eq.(21) and rewriting $\Delta\gamma_{oct}$ into γ_{oct}, one obtains

$$N_t \int_{\gamma_{oct,min.}}^{\gamma_{oct,max.}} \frac{p(\gamma_{oct})}{N_1} \left(\frac{\gamma_{oct}}{\gamma_{1oct}}\right)^{\frac{1}{\alpha}} d\gamma_{oct} = 1 \tag{23}$$

If the γ_{oct}~N relationship can be extended to the static test, Eq.(23) turns out as

$$4N_t \int_{\gamma_{oct,min.}}^{\gamma_{oct,max.}} p(\gamma_{oct}) \left(\frac{\gamma_{oct}}{2\gamma_{octf}}\right)^{\frac{1}{\alpha}} d\gamma_{oct} = 1 \tag{24}$$

With this equation, one can estimate the total number of cycles N_t. The experimental varification is not done yet.

Conclusions

The followings are concluded:

(1) The experimental results showed the linear relationship $\Delta\delta N^{0.24}=0.10$, for the uniaxial case, $\Delta\gamma_{xy} N^{0.34}=0.32$ for the torsional case, and $\Delta\gamma_{oct} N^{0.23}=0.13$ for the combined synchronous case on the log-log paper. However, the slopes of these lines were found to be more gentle than that by Coffin. The discrepancy may be because rather averaged strain was measured in this study.

(2) In the range of the number of cycles to fracture of more than one hundred, γ_{oct}~N relationship was found to coincide for all the test except the nonsynchronous test. In the cycle range lower than one hundred, the mode of fracture was different from that for the higher cycle range and it is so complicated that the above mentioned discrepancy may have appeared. For the lower cycle range, the data of the torsion test drop a little above those for other tests.

(3) The results of torsion test coincided with those of the bending test of oval plates and of the anticlastic bending test of rhombic plates.

(4) For the nonsynchronous test, it is suggested that other kind of parameter such as hysteresis energy per cycle should be used.

(5) For the random fatigue caused by earthquakes, it may be possible to calculate the probability density $p(\gamma_{oct})$ and then to determine the total number of cycles N_t by Eq.(23) or Eq.(24).

Acknowledgements

The author wishes to express his sincere gratitude to the late Professor Dr. Joseph Marin, Former Head of Engineering Mechanics Department at the Pennsylvavia State University, and Professor Dr. Kiyoshi Ban, Dean of the Faculty of Engineering at Kobe University, and Professor Dr. Yoshihisa Gyoten and other colleagues at Kobe University for their giving the chance to perform this investigation.

Bibliography

(1) Manson, S. S.: "Behavior of Materials under Conditions of Thermal Stress", NACA Tech. Note 2933, July, 1953.

(2) Benham, P. P.: "Fatigue of Metals Caused by a Relatively Few Cycles of High Load or Strain Amplitudes", Metallurgical Reviews, Vol. 3, No. 11, 1958.

(3) Yao, J. T. P. and W. H. Munse: "Low Cycle Fatigue of Metals, Literature Review", Welding Journal, Vol. 41, 1962.

(4) Coffin, L. F. Jr.: "Low Cycle Fatigue, A Review", Applied Material Research, Vol. 1, No. 3, 1962.

(5) Marin, J. and K. Ohji: "A Review of Research on Low Cycle Fatigue", The Pennsylvania State University, Aug., 1965.

(6) Richards, C. W.: "Engineering Materials Science", Wadsworth Publishing Co., Inc., 1961.

(7) Manson, S. S. and M. H. Hirschberg: "Fatigue Behavior in Strain Cycling in the Low and Intermediate Cycle Range", The Tenth Sagamore Army Materials Research Conference, Aug., 1963.

(8) Morrow, JoDean: "Cyclic Plastic Strain Energy and Fatigue of Metals", ASTM STP 378, 1965.

(9) Halford, G. R. and JoDean Morrow: "Low Cycle Fatigue in Torsion", Proc. of ASTM, Vol. 62, 1963.

(10) Goto, T.: M.S. Thesis, Engineering Mechanics Dept., The Pennsylvania State University, 1966.

(11) Shewchuk, J.: Ph.D. Thesis, Engineering Mechanics Dept., The Pennsylvania State University, 1966.

(12) Crandall, S. H.: "Random Vibration", Vol. 1, MIT Press, 1958.

(13) Schijve J.: "The Analysis of Random Load-Time Histories with Relation to Fatigue Tests and Life Calculations", Pergamon Press, 1963.

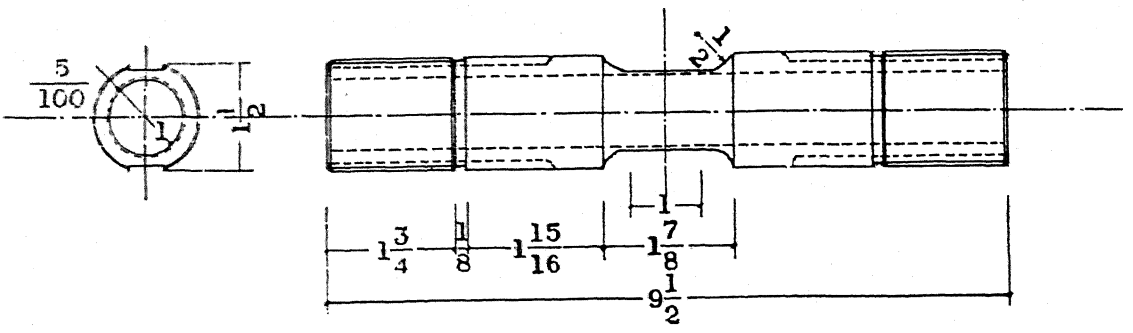

Fig. 1. Dimensions of Specimens (Unit: inch).

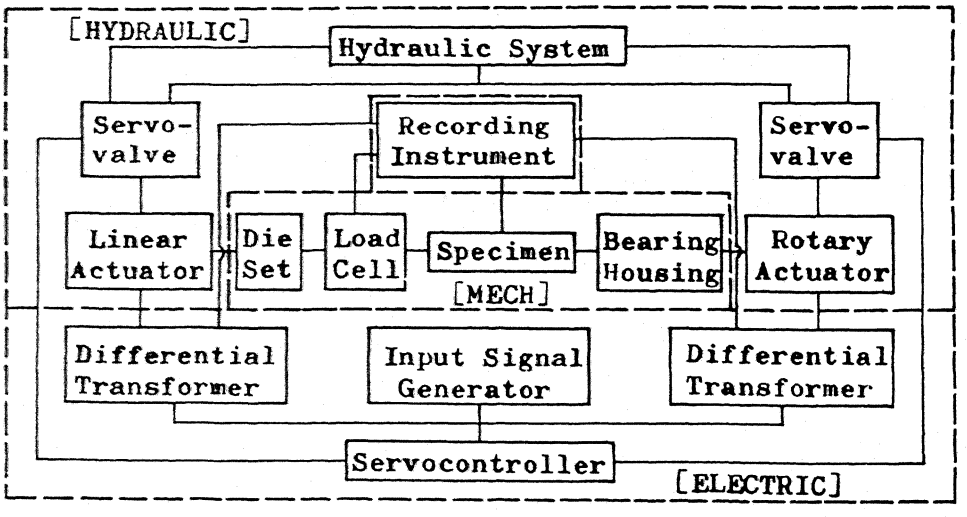

Fig. 2. Block Diagram of the Testing Machine.

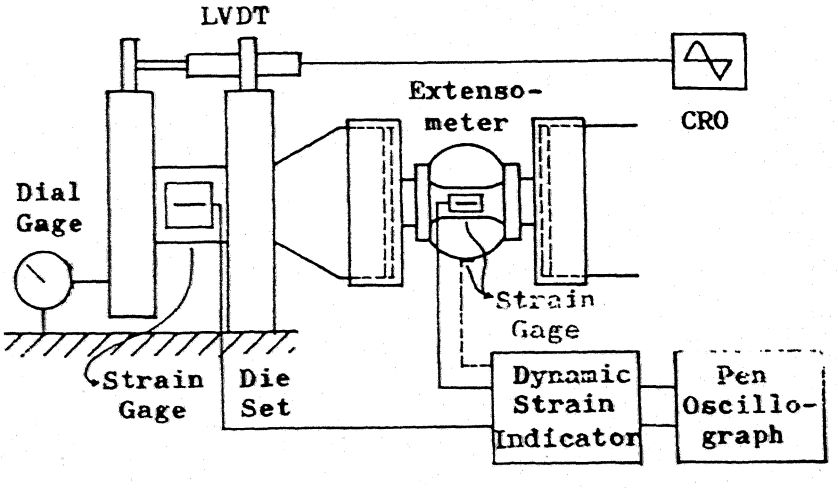

Fig. 3(a). Schematic Arrangement of Measuring Systems for Axial Motion.

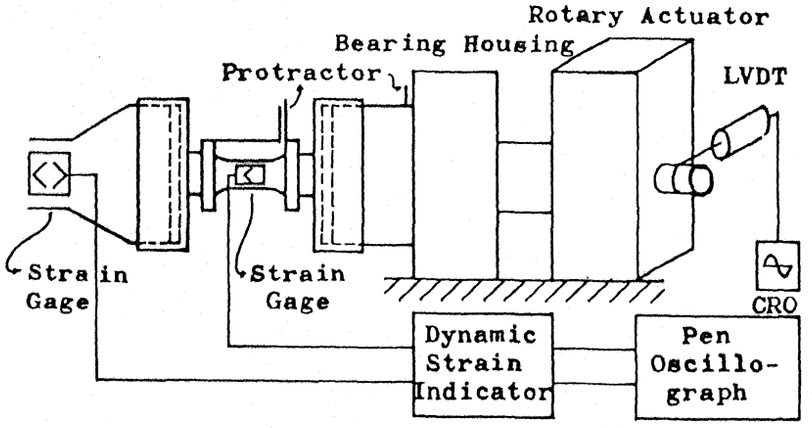

Fig. 3(b). Schematic Arrangement of Measuring Systems for Torsion.

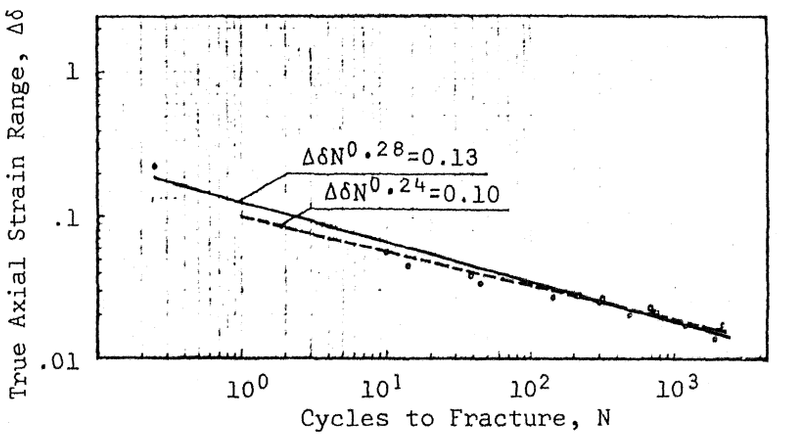

Fig. 4. True Axial Strain Range vs. the Number of Cycles to Fracture in the Uniaxial Test.

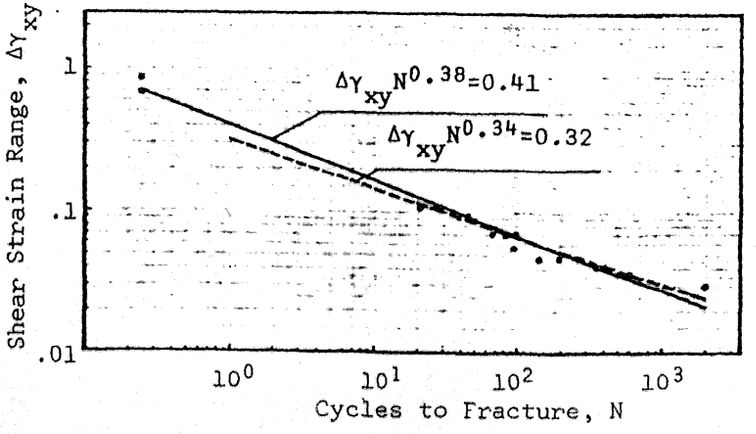

Fig. 5. Shear Strain Rainge vs. the Number of Cycles to Fracture in the Torsion Test.

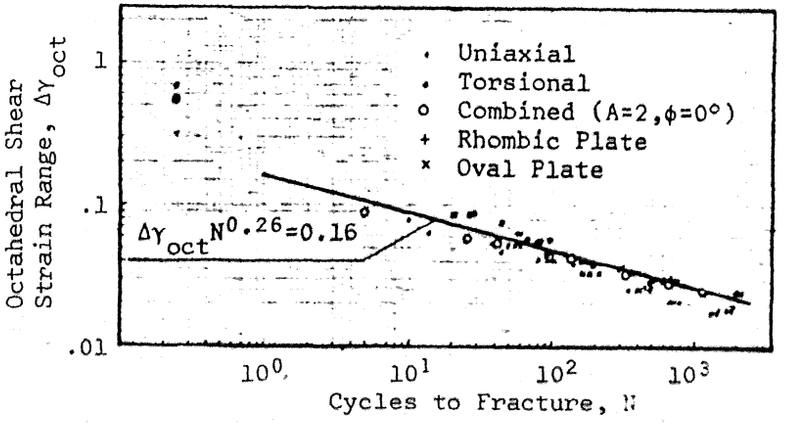

Fig. 6. Octahedral Shear Strain Range vs. the Number of Cycles Fracture for Various Strain Conditions

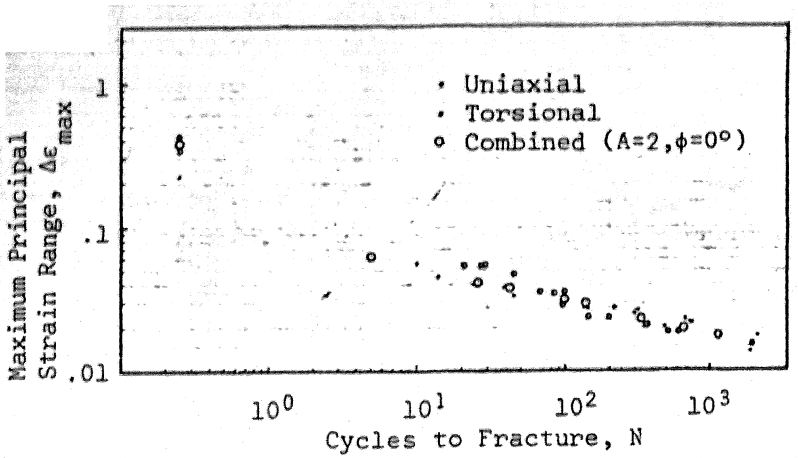

Fig. 7. Maximum Principal Strain Range vs. the Number of Cycles to Fracture for Various Strain Conditions.

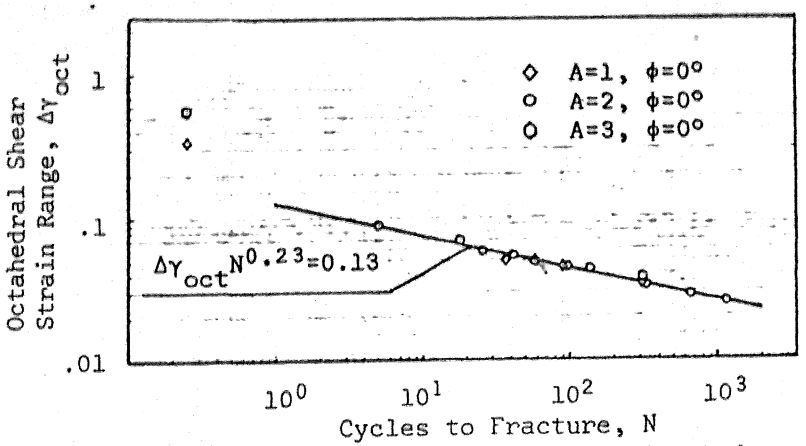

Fig. 8. Octahedral Shear Strain Range vs. the Number of Cycles to Fracture in the Combined Axial and Torsional Synchronous Test with Various Strain Ratios, $A=\frac{\Delta\gamma_{xy}}{\Delta\delta}$

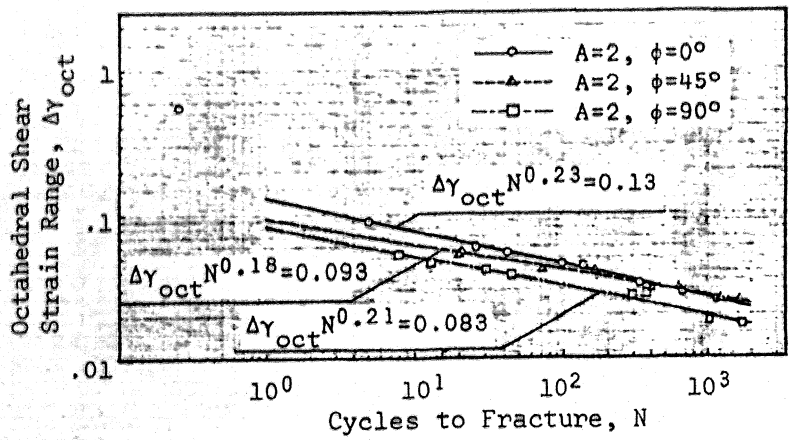

Fig. 9. Octahedral Shear Strain Range vs. the Number of Cycles to Fracture in the Combined Axial and Torsional Nonsynchronous Test.

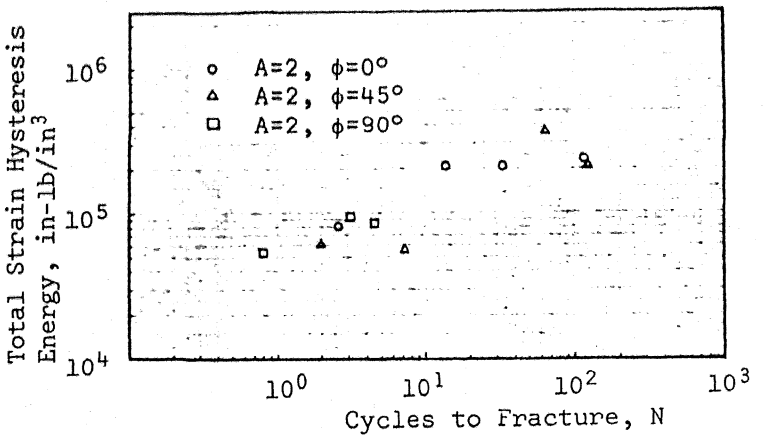

Fig. 10. Total Strain Hysteresis Energy vs. the Number of Cycles to Fracture in the Combined Axial and Torsional Nonsynchronous Test.